Center for Turbulence Research
Proceedings of the Summer Program 2006

Turbulence suppression in channel flows by means of a streamwise traveling wave

By M. R. Jovanović†, R. Moarref† AND D. You

We assess the effectiveness of using a zero-net-mass-flux blowing and suction in the form of an upstream traveling wave for transition control in channel flows. Our study is motivated by a recent paper by Min *et al.* (2006), where it was shown that this type of surface actuation yields a sustained sublaminar drag in a fully developed channel flow. We develop models that govern the dynamics of velocity fluctuations in the presence of stochastic outside disturbances (such as free-stream turbulence and acoustic waves) and show how changes in control parameters affect the fluctuations' kinetic energy density. Effectively, we establish that properly designed streamwise traveling waves can be used to weaken intensity of both the streamwise streaks and the Tollmien-Schlichting waves in transitional channel flows.

1. Introduction

Significant attention has recently been paid to the problem of turbulence suppression in channel flows using feedback control with wall-mounted arrays of sensors and actuators. This problem is viewed as a benchmark for skin-friction drag reduction in a variety of geometries, including boundary layers. Successful Linear Quadratic Regulator and Linear Quadratic Gaussian schemes have been designed and tested in direct numerical simulations (DNS) of nonlinear low-Reynolds-number flow dynamics (Bewley & Liu 1998; Lee *et al.* 2001; Kim 2003; Högberg *et al.* 2003*a*,*b*; Hoepffner *et al.* 2005; Chevalier *et al.* 2006). All of these studies are *model-based*; the linearized Navier-Stokes (NS) equations are used as a model for the flow dynamics and the modern control theory is utilized for a design of flow estimators and controllers.

An alternative approach to flow control relies on the understanding of the basic flow physics and the open-loop implementation of controls (i.e., without measurement of the relevant flow quantities and disturbances). Examples of the *physics-based sensorless* strategies include: wall geometry deformation such as riblets (Walsh 1983; Choi *et al.* 1993; Grek *et al.* 1996), transverse wall oscillations (Jung *et al.* 1992; Baron & Quadrio 1996; Orlandi & Fatica 1997), and control of conductive fluids using the Lorentz force (Berger *et al.* 2000; Du & Karniadakis 2000; Karniadakis & Choi 2003). Although several numerical and experimental studies show that *properly designed* sensorless strategies yield significant drag reduction, an obstacle to fully utilizing these physics-based approaches is the absence of a theoretical framework for their design and optimization.

An enormous potential of sensorless strategies was recently exemplified by Min *et al.* (2006), where a DNS study was used to show that a surface blowing and suction in the form of an upstream traveling wave gives a sustained sublaminar drag in a fully developed

† Department of Electrical and Computer Engineering, University of Minnesota, Minneapolis, MN 55455, USA (mihailo@umn.edu).

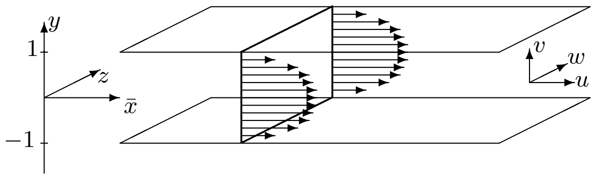

FIGURE 1. Three dimensional channel flow.

channel flow. The underlying mechanism for the sublaminar drag is the generation of the wall region Reynolds shear stresses of the opposite signs compared to what is expected based on the mean shear. By assuming that a surface actuation *only* influences the velocity fluctuations, Min *et al.* (2006) found an explicit solution to the two-dimensional linearized NS equations and showed that the drag is increased with the downstream traveling waves, and decreased with the upstream traveling waves.

An important open question is related to the dynamics of velocity fluctuations in the presence of the streamwise traveling waves. We address this problem by analyzing receptivity of the linearized NS equations in the presence of controls. It is shown that the properly designed surface actuation is capable of reducing receptivity of both the streamwise streaks and the Tollmien-Schlichting (TS) waves.

Our subsequent development is organized as follows: in Section 2 we determine a nominal velocity induced by a blowing and suction in the form of a streamwise traveling wave. In Section 3, we present an appropriate frequency representation of the linearized NS equations, and briefly discuss a notion of the *ensemble average energy density* of the statistical steady-state. A computationally efficient method for determination of the energy density in the presence of small amplitude traveling waves is described in Section 4. In Section 5, we employ perturbation analysis to identify the control parameters that reduce receptivity of the linearized equations. A brief summary of the main results is provided in Section 6.

2. Nominal velocity profile

Consider a channel flow governed by the non-dimensional incompressible NS equations

$$\begin{aligned} \mathbf{u}_{\bar{t}} &= -(\mathbf{u}\cdot\boldsymbol{\nabla})\,\mathbf{u} - \boldsymbol{\nabla}P + (1/R)\Delta\mathbf{u} + \mathbf{F}, \\ 0 &= \boldsymbol{\nabla}\cdot\mathbf{u}, \end{aligned} \tag{2.1}$$

with the Reynolds number defined in terms of maximal nominal velocity $\bar{U}_0$ and channel half-width δ, $R := \bar{U}_0\delta/\nu$. The kinematic viscosity is denoted by ν, the velocity vector is given by $\mathbf{u}$, P is the pressure, $\mathbf{F}$ is the body force, $\boldsymbol{\nabla}$ is the gradient, and $\Delta := \boldsymbol{\nabla}^2$ is the Laplacian. The spatial coordinates and time are represented by $(\bar{x}, \bar{y}, \bar{z})$ and $\bar{t}$, respectively, and the flow geometry is shown in Fig. 1.

Let us assume that in addition to a uniform streamwise pressure gradient, the flow is exposed to a zero-net-mass-flux surface blowing and suction in the form of a streamwise traveling wave. In the absence of the nominal body force, $\bar{\mathbf{F}} \equiv 0$, the nominal velocity $\bar{\mathbf{u}} := (U, V, W)$ represents a solution to Eq. (2.1) subject to

$$\begin{aligned} V(\bar{y} = \pm 1) &= \mp 2\,\alpha\,\cos(\omega_o(\bar{x} - c\,\bar{t})), \quad \bar{\mathbf{F}} \equiv 0, \\ U(\pm 1) = V_y(\pm 1) &= W(\pm 1) = 0, \quad \bar{P}_{\bar{x}} = -2/R, \end{aligned} \tag{2.2}$$

where α, ω_o, and c, respectively, denote amplitude, frequency, and speed of the streamwise traveling wave. Positive values of c define a wave moving in the downstream direction, while negative values of c define an upstream traveling wave.

The time dependence in $V(\pm 1)$ can be eliminated by the following coordinate transformation $\{x := \bar{x} - c\,\bar{t},\, y := \bar{y},\, z := \bar{z},\, t := \bar{t}\}$. This change of coordinates does not influence the spatial differential operators, but it transforms the time derivative to $\partial_{\bar{t}} = \partial_t - c\,\partial_x$, which adds an additional convective term to the NS equations

$$\begin{aligned} \mathbf{u}_t &= c\mathbf{u}_x - (\mathbf{u}\cdot\boldsymbol{\nabla})\,\mathbf{u} - \boldsymbol{\nabla}P + (1/R)\Delta\mathbf{u} + \mathbf{F}, \\ 0 &= \boldsymbol{\nabla}\cdot\mathbf{u}. \end{aligned} \tag{NS}$$

In the new coordinates, (2.1,2.2) exhibits a two-dimensional steady-state solution of the form $\bar{\mathbf{u}} = (U(x,y),\, V(x,y),\, 0) := (\Psi_y(x,y),\, -\Psi_x(x,y),\, 0)$, where stream function $\Psi(x,y)$ satisfies the following non-linear equation

$$\begin{aligned} &(1/R)\Delta^2\Psi + (c - \Psi_y)\,\Delta\Psi_x + \Psi_x\,\Delta\Psi_y = 0, \\ &\Psi(\pm 1) = \pm\mathrm{i}(\alpha/\omega_o)\,(\mathrm{e}^{-\mathrm{i}\omega_o x} - \mathrm{e}^{\mathrm{i}\omega_o x}),\ \Psi_y(\pm 1) = 0. \end{aligned} \tag{SF}$$

The solution to (SF) can be determined numerically using standard NS solvers. In this paper, however, we will consider a situation in which a surface blowing and suction has a small amplitude. For small values of α, we represent $\Psi(x,y)$ as

$$\Psi(x,y) := \Psi_0(y) + \sum_{l=1}^{\infty}\alpha^l\Psi_l(x,y),$$

and perform a perturbation analysis to efficiently solve (SF) and determine corrections to the nominal velocity in Poiseuille flow. In the above expansion, $\Psi_0'(y) := \Psi_{0y}(y) = U_0(y) = 1 - y^2$ denotes the plane channel flow, and $\Psi_l(x,y)$ represent the corrections to the nominal stream function caused by the surface blowing and suction. It turns out that $\Psi_l(x,y)$ can be represented as

$$\Psi_l(x,y) = \sum_{r \overset{2}{=} -l}^{l}\Psi_{l,r}(y)\mathrm{e}^{\mathrm{i}r\omega_o x},\quad l \geq 1,$$

where $\sum_{r \overset{2}{=} -l}^{l}$ signifies that r takes the values $\{-l, -l+2, \ldots, l-2, l\}$. Each $\Psi_{l,r}(y)$ is obtained as a solution to a linear ordinary differential equation derived by substituting the expression for $\Psi(x,y)$ in (SF) and matching the terms of equal powers in α. These equations are not presented here due to page constraints (they are to be reported elsewhere).

3. Linearized Navier-Stokes equations

We next present the constitutive equations describing the dynamics (up to a first order) of velocity fluctuations $\mathbf{v} := (u,\, v,\, w)$ around the nominal velocity profile of Section 2. These equations are obtained by decomposing each field in (NS) into the sum of a nominal and a fluctuating part, e.g., $\mathbf{u} := \bar{\mathbf{u}} + \mathbf{v}$, and by neglecting the quadratic terms in $\mathbf{v}$. A standard conversion to the wall-normal velocity (v)/vorticity (η) formulation removes the pressure from the equations and yields the following evolution model with *forcing*

$$\begin{aligned} E\,\boldsymbol{\psi}_t(x,y,z,t) &= F\,\boldsymbol{\psi}(x,y,z,t) + G\,\mathbf{d}(x,y,z,t), \\ \mathbf{v}(x,y,z,t) &= C\,\boldsymbol{\psi}(x,y,z,t). \end{aligned} \tag{LNS}$$

This evolution model is driven by the body force fluctuation vector $\mathbf{d} := (d_1,\, d_2,\, d_3)$, which can account for the outside flow disturbances such as acoustic waves or free-stream turbulence. These types of excitations are arguably present in most wall-bounded flow configurations and it is of interest to investigate their influence on velocity fluctuations. The internal state of (LNS) is determined by $\boldsymbol{\psi} := (v,\, \eta)$, with Dirichlet and Neumann boundary conditions on v and Dirichlet boundary conditions on η.

All operators in (LNS) are matrices of differential operators in three coordinate directions x, y, and z. We note that operator C in (LNS) captures a kinematic relationship between $\boldsymbol{\psi}$ and $\mathbf{v}$, operator G describes how outside disturbances enter into the evolution model, whereas operators E and F determine internal properties of the linearized equations (for example, stability). While operators E, G, and C do not depend on the nominal velocity, operator F is nominal velocity dependent and, hence, it determines changes in the dynamics due to changes in $\bar{\mathbf{u}}$. For the nominal velocity $\bar{\mathbf{u}} = (U(x,y),\, V(x,y),\, 0)$, F is a 2×2 block-operator with components

$$
\begin{aligned}
F^{11} &= \tfrac{1}{R}\Delta^2 + ((\Delta U) - (U - cI)\Delta)\partial_x - (\Delta V)\partial_y - V\Delta\partial_y - 2V_x\partial_{xy} + U_x(\Delta - 2\partial_{xx}) - \\
&\quad (\Delta V_y) + (2(\Delta V)\partial_x + \Delta V_x + V_x(\Delta - 2\partial_{yy}) - 2U_x\partial_{xy})\,(\partial_{xx} + \partial_{zz})^{-1}\partial_{xy},\\
F^{12} &= -\,(2(\Delta V)\partial_x + \Delta V_x + V_x(\Delta - 2\partial_{yy}) - 2U_x\partial_{xy})\,(\partial_{xx} + \partial_{zz})^{-1}\partial_z,\\
F^{21} &= -\left(U_y\partial_z + V_x(\partial_{xx} + \partial_{zz})^{-1}\partial_{yyz}\right),\\
F^{22} &= \tfrac{1}{R}\Delta - (U_x + (U - cI)\partial_x + V\partial_y) - V_x(\partial_{xx} + \partial_{zz})^{-1}\partial_{xy},
\end{aligned}
$$

where ∂_x, ∂_y, and ∂_z represent differential operators in x, y, and z, respectively, and $(\partial_{xx} + \partial_{zz})^{-1}$ is defined by

$$
(\partial_{xx} + \partial_{zz})^{-1} : f \mapsto g \;\;\Leftrightarrow\;\; f = (\partial_{xx} + \partial_{zz})g =: g_{xx} + g_{zz}.
$$

Moreover, for the nominal velocity presented in Section 2, F inherits spatial periodicity in x from $\bar{\mathbf{u}}$ and each of its components can be represented as

$$
F^{ij} = F_0^{ij} + \sum_{l=1}^{\infty} \alpha^l \sum_{r \stackrel{2}{=} -l}^{l} \mathrm{e}^{\mathrm{i}r\omega_o x} F_{l,r}^{ij},
$$

where F_0^{ij} and $F_{l,r}^{ij}$ are spatially invariant operators in the streamwise and spanwise directions. This expansion effectively isolates spatially invariant and spatially periodic parts of operator F, which is particularly well-suited for representation of (LNS) in the frequency domain.

3.1. *Frequency representation of the linearized model*

Owing to the structure of the linearized equations, differential operators E, G, and C are invariant with respect to translations in horizontal directions. On the other hand, operator F is (spatially) invariant in z and (spatially) periodic in x. Thus, the Fourier transform in z can be applied to algebraize the spanwise differential operators. In other words, the normal modes in z are the spanwise waves $\mathrm{e}^{\mathrm{i}k_z z}$, where k_z denotes the spanwise wave number. On the other hand, the appropriate normal modes in x are given by the so-called *Bloch waves* (Nayfeh & Mook 1979), which are determined by a product of $\mathrm{e}^{\mathrm{i}\theta x}$ and the $2\pi/\omega_o$ periodic function in x, with $\theta \in [0,\, \omega_o)$. Based on the above, each signal in (LNS) (for example, $\mathbf{d}$) can be expressed as

$$
\left.
\begin{aligned}
\mathbf{d}(x,y,z,t) &= \mathrm{e}^{\mathrm{i}k_z z}\mathrm{e}^{\mathrm{i}\theta x}\,\bar{\mathbf{d}}(x,y,k_z,t)\\
\bar{\mathbf{d}}(x,y,k_z,t) &= \bar{\mathbf{d}}(x + 2\pi/\omega_o, y, k_z, t)
\end{aligned}
\right\}\;\; k_z \in \mathbb{R},\;\; \theta \in [0,\, \omega_o),
$$

where only real parts are to be used for representation of physical quantities. Expressing $\bar{\mathbf{d}}(x, y, k_z, t)$ in its Fourier series finally yields

$$\mathbf{d}(x,y,z,t) \;=\; \sum_{n=-\infty}^{\infty} \bar{\mathbf{d}}_n(y,k_z,t)\,\mathrm{e}^{\mathrm{i}\theta_n x + \mathrm{i}k_z z}, \quad \begin{array}{l} \theta_n \;:=\; \theta + n\omega_o, \\ k_z \in \mathbb{R},\; \theta \in [0,\,\omega_o), \end{array} \tag{NM}$$

where $\{\bar{\mathbf{d}}_n(y,k_z,t)\}_{n\in\mathbb{Z}}$ are the coefficients in the Fourier series expansions of $\bar{\mathbf{d}}(x,y,k_z,t)$.

The frequency representation of the linearized NS equations is obtained by substituting (NM) into (LNS)

$$\begin{aligned} \partial_t \boldsymbol{\psi}_\theta(y,k_z,t) &= \mathcal{A}_\theta(k_z)\,\boldsymbol{\psi}_\theta(y,k_z,t) \;+\; \mathcal{B}_\theta(k_z)\,\mathbf{d}_\theta(y,k_z,t), \\ \mathbf{v}_\theta(y,k_z,t) &= \mathcal{C}_\theta(k_z)\,\boldsymbol{\psi}_\theta(y,k_z,t). \end{aligned} \tag{FR}$$

This representation is parameterized by $k_z \in \mathbb{R}$ and $\theta \in [0,\,\omega_o)$ and $\boldsymbol{\psi}_\theta(y,k_z,t)$ denotes a bi-infinite column vector, $\boldsymbol{\psi}_\theta(y,k_z,t) := \mathrm{col}\,\{\boldsymbol{\psi}(\theta_n,y,k_z,t)\}_{n\in\mathbb{Z}}$. The same definition applies to $\mathbf{d}_\theta(y,k_z,t)$ and $\mathbf{v}_\theta(y,k_z,t)$. On the other hand, for each k_z and θ, $\mathcal{A}_\theta(k_z)$, $\mathcal{B}_\theta(k_z)$, and $\mathcal{C}_\theta(k_z)$ are bi-infinite matrices whose elements are one-dimensional operators in y. The structure of these operators depends on frequency representation of E, F, G, and C in (LNS), and it can be determined using the following set of simple rules (Fardad, Jovanović & Bamieh 2005):

• A *spatially invariant* operator L with Fourier symbol $L(k_x)$ has a block-diagonal representation

$$\mathcal{L}_\theta \;:=\; \mathrm{diag}\,\{L(\theta_n)\}_{n\in\mathbb{Z}} \;=\; \begin{bmatrix} \ddots & \vdots & \vdots & \vdots & \iddots \\ \cdots & L(\theta_{n-1}) & 0 & 0 & \cdots \\ \cdots & 0 & L(\theta_n) & 0 & \cdots \\ \cdots & 0 & 0 & L(\theta_{n+1}) & \cdots \\ \iddots & \vdots & \vdots & \vdots & \ddots \end{bmatrix}.$$

For example, if $L = \partial_x$, then $\mathcal{L}_\theta = \mathrm{diag}\,\{\mathrm{i}(\theta + n\omega_o)\}_{n\in\mathbb{Z}}$. Operators E, G, C, F_0, and $F_{l,r}$ in (LNS) are spatially invariant and, thus, their representations are block-diagonal.

• A *spatially periodic function* $T(x)$ with Fourier series coefficients $\{T_n\}_{n\in\mathbb{Z}}$ has a θ-independent block-Toeplitz representation

$$\mathcal{T} \;:=\; \mathrm{toep}\left\{\cdots, T_2, T_1, \boxed{T_0}, T_{-1}, T_{-2}, \cdots\right\} \;=\; \begin{bmatrix} \ddots & \vdots & \vdots & \vdots & \iddots \\ \cdots & T_0 & T_{-1} & T_{-2} & \cdots \\ \cdots & T_1 & T_0 & T_{-1} & \cdots \\ \cdots & T_2 & T_1 & T_0 & \cdots \\ \iddots & \vdots & \vdots & \vdots & \ddots \end{bmatrix},$$

where the box denotes the element on the main diagonal of $\mathcal{T}$. For example, $T(x) = \mathrm{e}^{-\mathrm{i}rx}$ has a block-Toeplitz representation $\mathcal{T} := \mathcal{S}_r$ with only non-zero element $T_{-r} = I$.

• A representation of the sums and cascades of spatially periodic functions and spatially invariant operators is readily determined from these special cases. For example, a matrix representation of operator $\mathrm{e}^{-\mathrm{i}rx}\partial_x$ is given by $\mathcal{S}_r\,\mathrm{diag}\,\{\mathrm{i}(\theta + n\omega_o)\}_{n\in\mathbb{Z}}$.

Based on these, we get the following representations for $\mathcal{A}_\theta$, $\mathcal{B}_\theta$, and $\mathcal{C}_\theta$ in (FR)

$$\mathcal{A}_\theta \;:=\; \mathcal{E}_\theta^{-1}\mathcal{F}_\theta \;=\; \mathcal{E}_\theta^{-1}\mathcal{F}_{0\theta} \;+\; \sum_{l=1}^{\infty}\alpha^l \sum_{r \overset{2}{=} -l}^{l} \mathcal{E}_\theta^{-1}\mathcal{S}_{-r}\mathcal{F}_{l,r\theta} \;=:\; \mathcal{A}_{0\theta} \;+\; \sum_{l=1}^{\infty}\alpha^l\,\mathcal{A}_{l\theta},$$

$$\mathcal{B}_\theta \;:=\; \mathcal{E}_\theta^{-1}\,\mathcal{G}_\theta,\;\; \mathcal{G}_\theta \;:=\; \mathrm{diag}\,\{G(\theta_n)\}_{n\,\in\,\mathbb{Z}},\;\; \mathcal{C}_\theta \;:=\; \mathrm{diag}\,\{C(\theta_n)\}_{n\,\in\,\mathbb{Z}},$$

where we have used the fact that $\mathcal{E}_\theta := \mathrm{diag}\,\{E(\theta_n)\}_{n\,\in\,\mathbb{Z}}$ is an invertible operator. For convenience of later algebraic manipulations, we rewrite $\mathcal{A}_{l\theta}$ as $\mathcal{A}_{l\theta} := \sum_{r \overset{2}{=} -l}^{l} \mathcal{S}_{-r}\,\mathcal{A}_{l,r\theta}$ where $\mathcal{A}_{l,r\theta} \;:=\; \mathrm{diag}\,\{A_{l,r}(\theta_n)\}_{n\,\in\,\mathbb{Z}} \;=\; \mathrm{diag}\,\{E^{-1}(\theta_{n+r})\,F_{l,r}(\theta_n)\}_{n\,\in\,\mathbb{Z}}$. In other words, for a given $l \geq 1$ operator $\mathcal{A}_{l\theta}$ has non-zero blocks only on rth sub-diagonals with $r \in \{-l, -l+2, \ldots, l-2, l\}$. This particular structure of $\mathcal{A}_{l\theta}$ is exploited in energy amplification perturbation analysis that is presented in Section 4.

3.2. *Energy amplification of the linearized model*

The frequency representation (FR) contains a large amount of information about linearized dynamics. For example, this model can be used to assess stability properties of the underlying nominal flow condition: stability of the linearized system (LNS) is equivalent to the stability of operator $\mathcal{A}_\theta(k_z)$ for each pair (k_z, θ). However, since the transition in wall-bounded shear flows is not appropriately described by the stability properties of the linearized equations (Butler & Farrell 1992; Trefethen *et al.* 1993; Farrell & Ioannou 1993; Reddy & Henningson 1993; Bamieh & Dahleh 2001; Schmid & Henningson 2001; Jovanović 2004; Jovanović & Bamieh 2005), we perform a receptivity analysis of stochastically forced model (FR) to assess the effectiveness of the proposed control strategy. Namely, we set the initial conditions in (FR) to zero and study responses of the linearized dynamics to uncertain body forces. When the body forces are absent, the response of stable flows eventually decays to zero. However, in the presence of stochastic body forces, the linearized NS equations are capable of maintaining high levels of the steady-state variance (Farrell & Ioannou 1993; Bamieh & Dahleh 2001; Jovanović 2004; Jovanović & Bamieh 2005). Our analysis quantifies the effect of imposed streamwise traveling waves on the asymptotic levels of variance and describes how receptivity changes in the presence of control. In Section 5, we illustrate how this approach can be utilized to provide systematic guidelines for a selection of control parameters.

Let us assume that a stable system (FR) is subject to a zero-mean white stochastic process (in y and t) $\mathbf{d}_\theta(y, k_z, t)$. Then, for each k_z and θ, the *ensemble average energy density* of the statistical steady-state is determined by

$$\bar{\mathrm{E}}(\theta, k_z) \;=\; \mathrm{trace}\left(\lim_{t\,\to\,\infty} \mathcal{E}\left\{\mathbf{v}_\theta(\cdot, k_z, t) \otimes \mathbf{v}_\theta(\cdot, k_z, t)\right\}\right),$$

where $\mathcal{E}$ is the expectation operator, and $\mathbf{v}_\theta \otimes \mathbf{v}_\theta$ denotes the tensor product of $\mathbf{v}_\theta$ with itself. We note that $\bar{\mathrm{E}}(\theta, k_z)$ determines the asymptotic level of variance maintained by a stochastic outside forcing in (FR). Typically, this quantity is computed by running the DNS of the NS equations until the statistical steady-state is reached. However, for the linearized system (FR), kinetic energy density $\bar{\mathrm{E}}(\theta, k_z)$ can be determined using the solution to the following operator Lyapunov equation (Fardad *et al.* 2005)

$$\mathcal{A}_\theta(k_z)\mathcal{P}_\theta(k_z) \;+\; \mathcal{P}_\theta(k_z)\mathcal{A}_\theta^*(k_z) \;=\; -\,\mathcal{B}_\theta(k_z)\mathcal{B}_\theta^*(k_z), \tag{LE}$$

as

$$\bar{\mathrm{E}}(\theta, k_z) \;=\; \mathrm{trace}\left(\mathcal{P}_\theta(k_z)\,\mathcal{C}_\theta^*(k_z)\,\mathcal{C}_\theta(k_z)\right),$$

where $\mathcal{P}_\theta(k_z)$ denotes the correlation operator of $\boldsymbol{\psi}_\theta$, that is

$$\mathcal{P}_\theta(k_z) \;:=\; \lim_{t\,\to\,\infty} \mathcal{E}\left\{\boldsymbol{\psi}_\theta(\cdot,k_z,t)\otimes\boldsymbol{\psi}_\theta(\cdot,k_z,t)\right\}.$$

Since $\mathcal{C}_\theta^*(k_z)\,\mathcal{C}_\theta(k_z)$ is an identity operator, we have $\bar{\mathrm{E}}(\theta,k_z) = \mathrm{trace}\left(\mathcal{P}_\theta(k_z)\right)$, and the total ensemble average energy is obtained by integration over θ and k_z

$$\begin{aligned}
\mathrm{E} \;&=\; \frac{1}{(2\pi)^2}\int_{-\infty}^{\infty}\int_0^{\omega_o} \mathrm{trace}\left(\mathcal{P}_\theta(k_z)\right)\,\mathrm{d}\theta\,\mathrm{d}k_z \\
&=\; \frac{1}{(2\pi)^2}\int_{-\infty}^{\infty}\sum_{n\,=\,-\infty}^{\infty}\int_0^{\omega_o} \mathrm{trace}\left(P_d(\theta_n,k_z)\right)\,\mathrm{d}\theta\,\mathrm{d}k_z \\
&=\; \frac{1}{(2\pi)^2}\int_{-\infty}^{\infty}\int_{-\,\infty}^{\infty} \bar{\mathrm{E}}(k_x,k_z)\,\mathrm{d}k_x\,\mathrm{d}k_z,
\end{aligned}$$

where $P_d(\theta_n,k_z)$ denote elements on the main diagonal of operator $\mathcal{P}_\theta$, and $\bar{\mathrm{E}}(k_x,k_z) := \mathrm{trace}\left(P_d(k_x,k_z)\right)$. We have arrived at the above expression for E using the fact that $\mathcal{P}_\theta(k_z)$ denotes a frequency representation of a spatially periodic operator, and a simple observation that as n and θ vary over $\mathbb{Z}$ and $[0,\,\omega_o)$, respectively, $k_x \,=\, \theta_n \,=\, \theta \,+\, n\omega_o$ assumes all values in $\mathbb{R}$ (Fardad *et al.* 2005; Fardad & Bamieh 2005). The last expression for the kinetic energy density, i.e., $\bar{\mathrm{E}}(k_x,k_z) := \mathrm{trace}\left(P_d(k_x,k_z)\right)$, is particularly convenient for comparison between the energy amplification of the uncontrolled and controlled flow systems.

4. Perturbation analysis of energy amplification

Solving (LE) is an arduous undertaking; a discretization of the operators (in y) and truncation of bi-infinite matrices converts (LE) into a large-scale matrix Lyapunov equation. However, since we want to quantify changes in energy amplification with control parameters, as well as with the spatial frequencies, determining even the solution to this approximation to (LE) is computationally expensive. Instead, we employ an efficient perturbation analysis based approach for solving (LE) (Fardad & Bamieh 2005). This method is well suited for systems with small amplitude spatially periodic terms, and it results in a set of equations with a convenient structure. Namely, the energy amplification can be computed by solving a conveniently coupled system of operator valued Lyapunov and Sylvester equations. A finite dimensional approximation of these equations yields a set of algebraic matrix equations whose order is determined by the size of discretization in y.

THEOREM 1. *Up to a second order in perturbation parameter α, the ensemble average energy density of system (LNS) is given by*

$$\begin{aligned}
\bar{\mathrm{E}}(k_x,k_z) \;&=\; \mathrm{trace}\;(X(k_x,k_z)) \,+\, \alpha^2\mathrm{trace}\;(Z(k_x,k_z)) \,+\, O(\alpha^4) \\
&=:\; \bar{\mathrm{E}}_0(k_x,k_z) \,+\, \alpha^2\bar{\mathrm{E}}_2(k_x,k_z) \,+\, O(\alpha^4),
\end{aligned}$$

where X and Z solve the following system of Lyapunov and Sylvester equations

$$\begin{aligned}
A_0(\theta_n)\,X(\theta_n) \,+\, X(\theta_n)\,A_0^*(\theta_n) \;&=\; -B(\theta_n)\,B^*(\theta_n), \\
A_0(\theta_{n-1})\,Y(\theta_n) \,+\, Y(\theta_n)\,A_0^*(\theta_n) \;&=\; -\left(A_{1,-1}(\theta_n)\,X(\theta_n) \,+\, X(\theta_{n-1})\,A_{1,1}^*(\theta_{n-1})\right), \\
A_0(\theta_n)\,Z(\theta_n) \,+\, Z(\theta_n)\,A_0^*(\theta_n) \;&=\; -\big(A_{2,0}(\theta_n)\,X(\theta_n) \,+\, X(\theta_n)\,A_{2,0}^*(\theta_n) \,+ \\
&\qquad A_{1,1}(\theta_{n-1})\,Y(\theta_n) \,+\, Y^*(\theta_n)\,A_{1,1}^*(\theta_{n-1}) \,+ \\
&\qquad A_{1,-1}(\theta_{n+1})\,Y^*(\theta_{n+1}) \,+\, Y(\theta_{n+1})\,A_{1,-1}^*(\theta_{n+1})\big)\,.
\end{aligned}$$

Remark 1. *Notation θ_{n-l} in Theorem 1 represents a shortcut for $k_x - l\omega_o$, i.e., $\theta_{n-l} := \theta + (n-l)\omega_o = \theta_n - l\omega_o = k_x - l\omega_o$. Furthermore, in the system of Lyapunov and Sylvester equations for X and Z we have slightly abused the notation by suppressing the dependence on k_z, e.g. $Y(\theta_{n+1}) = Y(\theta_{n+1}, k_z) = Y(k_x + \omega_o, k_z)$.*

Remark 2. *The expression for the ensemble average energy density in Theorem 1 can be generalized to account for higher order corrections in α. It turns out that only terms of even powers in α contribute to $\bar{\mathrm{E}}$, which in controlled flows depends on six parameters,*

$$\bar{\mathrm{E}}(k_x, k_z, R, \alpha, \omega_o, c) \;=\; \bar{\mathrm{E}}_0(k_x, k_z, R) \;+\; \sum_{l\,=\,1}^{\infty} \alpha^{2l} \bar{\mathrm{E}}_{2l}(k_x, k_z, R, \omega_o, c). \qquad \text{(ED)}$$

Since our objective is to identify trends in energy amplification, we confine our attention to a perturbation analysis up to a second order in α. We briefly comment on the influence of higher order corrections to the energy amplification in Section 5, where we show that the trends are correctly predicted by a perturbation analysis up to a second order.

5. Energy amplification in Poiseuille flow with $R = 2000$

In this Section, we study the energy amplification of stochastically excited linearized model. Theorem 1 reveals the dependence of the ensemble average energy density on the traveling wave amplitude α, for $0 < \alpha \ll 1$. However, since the operators in (FR) depend on the spatial wavenumbers, the Reynolds number R, the wave frequency ω_o, and the wave speed c, the energy amplification is also a function of these parameters. We discuss how the energy amplification changes with these parameters in plane channel flow with $R = 2000$, and demonstrate that the streamwise traveling waves of properly selected frequency and speed have a potential for reducing receptivity. We also underline some of the basic tradeoffs that need to be addressed in the process of selecting control parameters.

5.1. *Energy amplification of uncontrolled flow*

We next briefly comment on the energy amplification in uncontrolled Poiseuille flow with $R = 2000$. For an in-depth treatment of this problem, see Jovanović (2004); Jovanović & Bamieh (2005).

Figure 2(a) illustrates the dependence of the uncontrolled ensemble average energy density on horizontal wavenumbers $\bar{\mathrm{E}}_0(k_x, k_z)$. This plot shows that the low streamwise wavenumbers and $O(1)$ spanwise wavenumbers carry most of the uncontrolled flow energy. The largest value of $\bar{\mathrm{E}}_0(k_x, k_z)$ occurs at ($k_x = 0$, $k_z \approx 1.78$), which means that the most amplified structures are infinitely elongated in the streamwise direction and have the spanwise length scale of approximately 3.5δ, where δ is the channel half-width. We note that these input-output resonances do not correspond to the least-stable modes of the linearized equations. Rather, they arise due to the coupling from the wall-normal velocity v to the wall-normal vorticity η. Physically, this coupling is a product of the vortex stretching (vortex tilting, lift-up) mechanism (Landahl 1975, 1980); the nominal shear is tilted in the wall-normal direction by the spanwise changes in v, which lead to a transient amplification of η. This mechanism does not take place either when the nominal shear is zero (i.e., $U' = 0$), or when there are no spanwise variations in v (i.e., $k_z = 0$). On

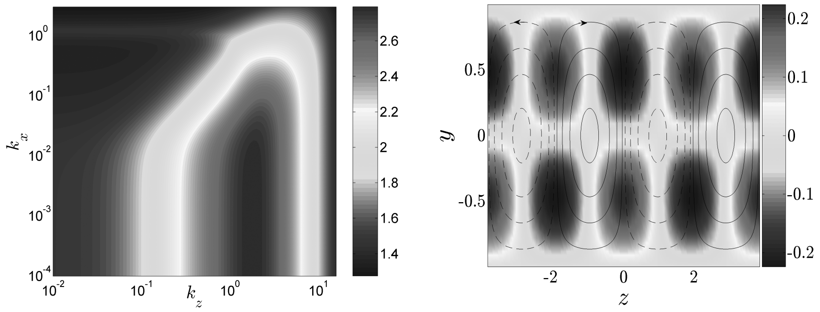

(a) (b)

Figure 2. (a) The ensemble average energy density $\bar{\mathrm{E}}_0(k_x, k_z)$ in uncontrolled flow with $R = 2000$. The plot is given in the log-log-log scale. (b) Flow structures that contain most energy in uncontrolled flow with $\{R = 2000,\ k_x = 0,\ k_z = 1.78\}$. The shaded plots represent streamwise velocity fluctuations and the contour lines represent stream function fluctuations.

the other hand, the least-stable modes of (LNS) create a local peak in $\bar{\mathrm{E}}_0(k_x, k_z)$ around $(k_z = 0,\ k_x \approx 1.2)$, with a magnitude significantly lower compared to the magnitude achieved by the streamwise constant flow structures.

Flow structures that contain the most energy in uncontrolled plane channel flow with $\{R = 2000,\ k_x = 0,\ k_z = 1.78\}$ are shown in Fig. 2(b). The shaded plots represent streamwise velocity and the contour lines represent stream function. The most amplified set of fluctuations results in pairs of counter-rotating streamwise vortices that generate high- and low-speed streaks antisymmetric with respect to the channel's centerline. These structures are ubiquitous in both experimental and numerical studies related to transition in channel and boundary layer flows. Thus, it is of interest to design a control strategy capable of weakening the energy content of streamwise constant velocity fluctuations.

5.2. *Energy amplification of controlled flow*

In this Section, we use Theorem 1 to show how blowing/suction in the form of a streamwise traveling wave influences amplification of stochastic outside disturbances in (LNS). We demonstrate that a judicious selection of wave frequency and speed can reduce receptivity. We also discuss some of the basic tradeoffs that need to be considered when selecting control parameters for turbulence suppression.

For a fixed Reynolds number, $\bar{\mathrm{E}}_0$ is just a function of k_x and k_z and it can be easily visualized as in Fig. 2(a). On the other hand, $\bar{\mathrm{E}}_2$ depends on four parameters (k_x, k_z, c, ω_o), which somewhat complicates the visualization process. Here, we analyze the cross-sections of $\bar{\mathrm{E}}_2(k_x, k_z, c, \omega_o)$ by fixing the values of ω_o and one of the wavenumbers. A complete parametric study of the contribution of $\bar{\mathrm{E}}_2$ to the kinetic energy density will be reported elsewhere.

Since most amplification in the uncontrolled flow occurs at $k_x = 0$, it is relevant to first study the influence of controls on the streamwise constant fluctuations. The uncontrolled kinetic energy density at $k_x = 0$ is shown in Fig. 3(a), where we observe a characteristic peak in $\bar{\mathrm{E}}_0(k_z)$ at $k_z \approx 1.78$. This peak determines the most energetic structures in the velocity field excited by a broadband, stochastic input field $\mathbf{d}$. On the other hand, Fig. 3(b) illustrates the dependence of $\bar{\mathrm{E}}_2$ on k_z and c for the streamwise constant fluctuations with $\omega_o = 0.01$. As evident from this plot, the wave speed c determines whether

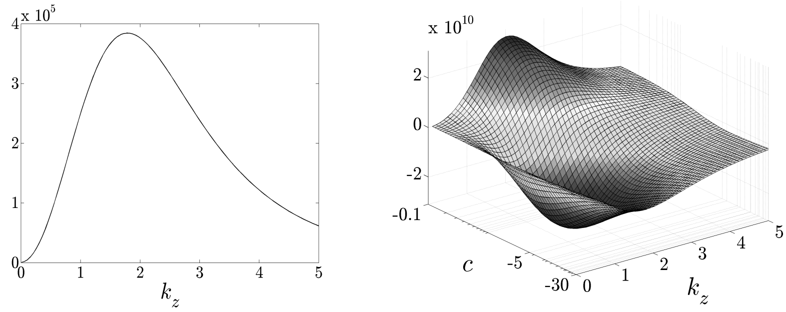

(a) (b)

FIGURE 3. (a) The ensemble average energy density $\bar{\mathrm{E}}_0(k_z)$ in uncontrolled flow with $\{R = 2000, k_x = 0\}$. (b) The second-order correction $\bar{\mathrm{E}}_2(k_z, c)$ to the ensemble average energy density in controlled flow with $\{R = 2000, k_x = 0, \omega_o = 0.01\}$.

surface blowing and suction amplifies or attenuates the most energetic components of the uncontrolled flow. We observe the variance attenuation for a fairly broad range of negative wave speeds, with the largest attenuation occurring for upstream traveling waves with $c \approx -2.655$. This value of c represents the wave speed that provides the largest variance suppression (up to a second order in α) of streamwise constant fluctuations in plane channel flow with $R = 2000$ and $\omega_o = 0.01$. On the other hand, the downstream waves and the low-speed upstream waves amplify variance of the uncontrolled flow. Note that the largest negative contributions of $\bar{\mathrm{E}}_2$ to the ensemble average energy density take place in the region of k_z's where function $\bar{\mathrm{E}}_0(k_z)$ peaks. This indicates that the upstream traveling waves introduce resonant interactions with the most energetic modes of the uncontrolled flow. The details of the underlying physical mechanisms that lead to a parametric resonance are deferred to a future study.

The above analysis illustrates the ability of the streamwise traveling waves to weaken the intensity of the most energetic modes of the uncontrolled flow. However, an important aspect in the evaluation of any control strategy is to consider the influence of controls on all of the system's modes. In view of this, we next discuss how control affects the spanwise constant fluctuations and the full three-dimensional fluctuations.

Figure 4(a) shows the energy density of the uncontrolled flow with $k_z = 0$. The peak in $\bar{\mathrm{E}}_0(k_x)$ at $k_x \approx 1.2$ is caused by the least-stable linearized modes, and the corresponding flow structures (TS waves) carry much less energy than the streamwise constant modes (cf. Fig. 3(a)). Figure 4(b) shows $\bar{\mathrm{E}}_2(k_x, c)$ for the traveling waves with $\omega_o = 0.01$. Note that the regions with negative and positive contributions to $\bar{\mathrm{E}}$ have changed compared to the streamwise constant case. In particular, the wave speed that provides the largest variance suppression at $k_x = 0$ increases the variance of the TS waves. In order to reduce the energy content of the TS waves, the speed of the upstream traveling waves needs to be increased. We observe that $c \approx -20$ provides variance suppression of both the streamwise streaks and the TS waves.

Figures 5(a) and 5(b), respectively, show the ensemble average energy densities of the full three-dimensional fluctuations in the uncontrolled and controlled flows with $\{R = 2000, \omega_o = 0.01, c = -20\}$. These plots demonstrate that the properly designed streamwise traveling waves are capable of reducing the energy content of the uncontrolled

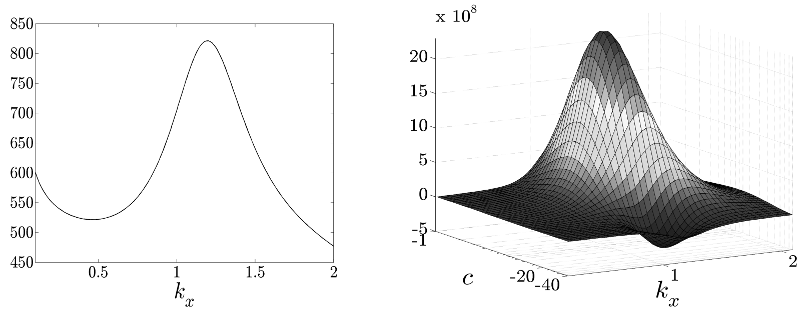

(a) (b)

FIGURE 4. (a) The ensemble average energy density $\bar{\mathrm{E}}_0(k_x)$ in uncontrolled flow with $\{R = 2000, k_z = 0\}$. (b) The second-order correction $\bar{\mathrm{E}}_2(k_x, c)$ to the ensemble average energy density in controlled flow with $\{R = 2000,\ k_z = 0,\ \omega_o = 0.01\}$.

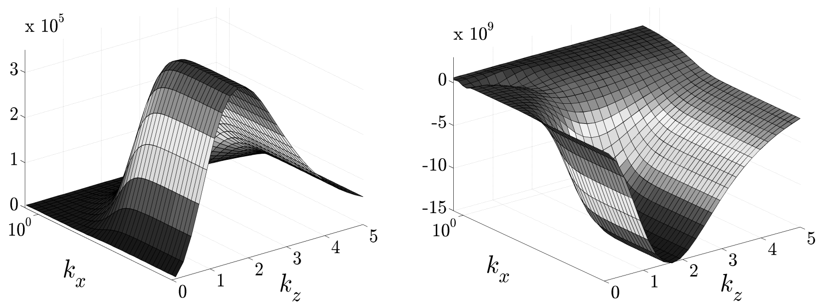

(a) (b)

FIGURE 5. (a) The ensemble average energy density $\bar{\mathrm{E}}_0(k_x, k_z)$ in uncontrolled flow with $R = 2000$. (b) The second-order correction $\bar{\mathrm{E}}_2(k_x, k_z)$ to the ensemble average energy density in controlled flow with $\{R = 2000,\ \omega_o = 0.01,\ c = -20\}$.

modes for all k_x and k_z. Furthermore, we observe that the regions representing large positive values of $\bar{\mathrm{E}}_0$ in Fig. 5(a) almost overlap with the regions representing large negative values of $\bar{\mathrm{E}}_2$ in Fig. 5(b). Therefore, the surface blowing and suction reduces the energy density of the uncontrolled flow for wavenumbers where $\bar{\mathrm{E}}_0(k_x, k_z)$ achieves its largest values. Thus, if the perturbation analysis (up to a second order in α) were to be used as a basis for the selection of control parameters (in the plane channel flow with $R = 2000$ and $\omega_o = 0.01$), the wave speed $c \approx -20$ would be a reasonable choice. However, we note that the stability of (LNS) will ultimately determine how much α can be increased before destabilizing the equations, which is an important parameter for choosing (α, ω_o, c). The analysis of stability properties is outside the scope of this work.

Figures 6(a) and 6(b) show the energy density of the uncontrolled flow (dotted curve) with $\{R = 2000,\ k_x = 0\}$, as well as the energy densities of the flows subject to the surface blowing and suction in the form of a streamwise traveling wave with $\{\omega_o = 0.01, c = -20\}$, $\alpha = 5/2000$ (Fig. 6(a)), and $\alpha = 8/2000$ (Fig. 6(b)). The controlled flow

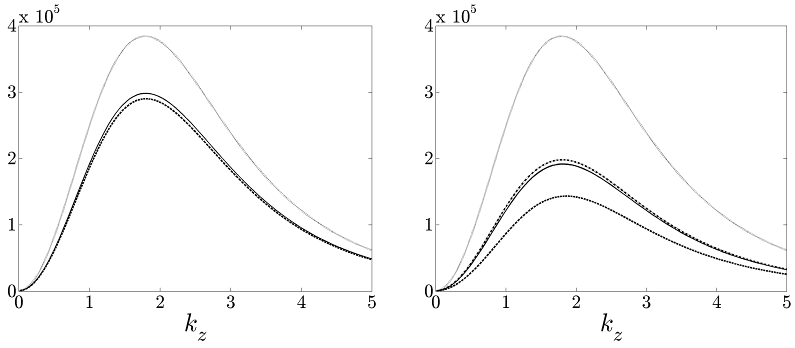

(a) (b)

FIGURE 6. The ensemble average energy densities $\bar{\mathrm{E}}(k_z)$ in the uncontrolled (dotted curve) and controlled flows with $\{R = 2000,\ k_x = 0,\ \omega_o = 0.01,\ c = -20\}$, and: (a) $\alpha = 5/2000$, (b) $\alpha = 8/2000$. The controlled flow plots are obtained by approximating the infinite summations in (ED) by the summations with: 1 (dashed curves), 2 (dot-dashed curves), 3 (solid curves), and 4 (solid curves) terms, respectively.

plots are obtained using perturbation analysis by approximating the infinite summations in (ED) by the summations with: one term (dashed curves), two terms (dot-dashed curves), three terms (solid curves), and four terms (solid curves), respectively. Clearly, for selected values of the traveling wave parameters, the approximations of $\bar{\mathrm{E}}$ in the controlled flows converge in both cases. We note that these results closely match the results obtained using large-scale computations. It is remarkable that the traveling waves of amplitudes equal to only 0.5 % and 0.8 % of the maximal nominal velocity ($\alpha = 5/2000$ and $\alpha = 8/2000$) are capable of suppressing the largest variance of the uncontrolled flow by approximately 23 % and 50 %, respectively. Furthermore, it is noteworthy that the second-order correction to the energy density captures the essential trends reflecting how much variance can be suppressed in the presence of controls.

6. Concluding remarks

This paper represents a continuation of recent efforts (Jovanović 2006; Moarref & Jovanović 2006) to develop a *model-based* approach for a design of *sensorless flow control strategies* in wall-bounded shear flows. The proposed method uses a receptivity analysis of the linearized NS equations as a basis for a selection of control parameters for turbulence suppression. The proposed framework avoids the need for the DNS/experiments in the early design stages and is capable of predicting the essential trends in a computationally efficient manner.

The new model-based design paradigm represents a spatial analog of the well-known principle of *vibrational control* (Meerkov 1980), where the system's dynamical properties are altered by introducing zero-mean oscillations into the system's coefficients. Depending on the relationship between the natural modes of the uncontrolled system and the forcing frequency, the vibrational control may have a potential for providing stability of the overall system and for changing its receptivity. For example, it is well known that the inverted pendulum can be stabilized by sensorless means using high frequency oscillations of the suspension point (Meerkov 1980). We show that the principle of vibrational control can be also utilized in systems governing the dynamics of flow fluctuations in channel flows, where coefficients multiplying the system's state have spatial periodicity. The key observation is that there is a potential for changing dynamical properties of the linearized NS equations (in favorable or unfavorable manner) whenever controls with spatial periodicity enter into the system's coefficients.

Acknowledgments

Part of this work was performed during the 2006 Center for Turbulence Research Summer Program with financial support from Stanford University and NASA Ames Research Center. The first author would like to thank Prof. P. Moin for creating an inspiring intellectual atmosphere and Dr. D. You for his hospitality during the stay. M. R. Jovanović's work was partially supported by the University of Minnesota start-up funds and R. Moarref's work was supported by the Office of the Dean of the Graduate School of the University of Minnesota Grant-in-Aid of Research, Artistry and Scholarship Award 1546-522-5985.

REFERENCES

Bamieh, B. & Dahleh, M. 2001 Energy amplification in channel flows with stochastic excitation. *Phys. Fluids* **13** (11), 3258–3269.

Baron, A. & Quadrio, M. 1996 Turbulent drag reduction by spanwise wall oscillations. *Appl. Sci. Res.* **55** (4), 311–326.

Berger, T. W., Kim, J., Lee, C. & Lim, J. 2000 Turbulent boundary layer control utilizing the Lorentz force. *Phys. Fluids* **12** (3), 631–649.

Bewley, T. R. & Liu, S. 1998 Optimal and robust control and estimation of linear paths to transition. *J. Fluid Mech.* **365**, 305–349.

Butler, K. M. & Farrell, B. F. 1992 Three-dimensional optimal perturbations in viscous shear flow. *Phys. Fluids A* **4**, 1637.

Chevalier, M., Hoepffner, J., Bewley, T. & Henningson, D. 2006 State estimation in wall-bounded flow systems. Part 2. Turbulent flows. *J. Fluid Mech.* **552**, 167–187.

Choi, H., Moin, P. & Kim, J. 1993 Direct numerical simulation of turbulent flow over riblets. *J. Fluid Mech.* **255**, 503–539.

Du, Y. & Karniadakis, G. E. 2000 Suppressing wall turbulence by means of a transverse traveling wave. *Science* **288**, 1230–1234.

Fardad, M. & Bamieh, B. 2005 A perturbation approach to the H_2 analysis of spatially periodic systems. In *Proceedings of the 2005 American Control Conference*, pp. 4838–4843. Portland, OR.

Fardad, M., Jovanović, M. R. & Bamieh, B. 2005 Frequency analysis and norms of distributed spatially periodic systems. *IEEE Transactions on Automatic Control* Submitted.

Farrell, B. F. & Ioannou, P. J. 1993 Stochastic forcing of the linearized Navier-Stokes equations. *Phys. Fluids A* **5** (11), 2600–2609.

Grek, G. R., Kozlov, V. V. & Titarenko, S. V. 1996 An experimental study of the influence of riblets on transition. *J. Fluid Mech.* **315**, 31–49.

Hoepffner, J., Chevalier, M., Bewley, T. & Henningson, D. 2005 State estimation in wall-bounded flow systems. Part 1. Perturbed laminar flows. *J. Fluid Mech.* **534**, 263–294.

Högberg, M., Bewley, T. R. & Henningson, D. S. 2003*a* Linear feedback control and estimation of transition in plane channel flow. *J. Fluid Mech.* **481**, 149–175.

Högberg, M., Bewley, T. R. & Henningson, D. S. 2003*b* Relaminarization of $R_{e\tau} = 100$ turbulence using linear state-feedback control. *Phys. Fluids* **15** (11), 3572–3575.

Jovanović, M. R. 2004 Modeling, analysis, and control of spatially distributed systems. PhD thesis, University of California, Santa Barbara.

Jovanović, M. R. 2006 Turbulence suppression in channel flows by small amplitude transverse wall oscillations. *Physics of Fluids* Submitted.

Jovanović, M. R. & Bamieh, B. 2005 Componentwise energy amplification in channel flows. *J. Fluid Mech.* **534**, 145–183.

Jung, W., Mangiavacchi, N. & Akhavan, R. 1992 Suppression of turbulence in wall-bounded flows by high-frequency spanwise oscillations. *Phys. Fluids A* **4** (8), 1605–1607.

Karniadakis, G. & Choi, K.-S. 2003 Mechanisms on transverse motions in turbulent wall flows. *Ann. Rev. Fluid Mech.* **35**, 45–62.

Kim, J. 2003 Control of turbulent boundary layers. *Phys. Fluids* **15** (5), 1093–1105.

Landahl, M. T. 1975 Wave breakdown and turbulence. *SIAM J. Appl. Math.* **28**, 735–756.

Landahl, M. T. 1980 A note on an algebraic instability of inviscid parallel shear flows. *J. Fluid Mech.* **98**, 243–251.

Lee, K. H., Cortelezzi, L., Kim, J. & Speyer, J. 2001 Application of reduced-order controller to turbulent flows for drag reduction. *Phys. Fluids* **13** (5), 1321–1330.

Meerkov, S. M. 1980 Principle of vibrational control: theory and applications. *IEEE Trans. Autom. Control* **AC-25** (4), 755–762.

Min, T., Kang, S. M., Speyer, J. L. & Kim, J. 2006 Sustained sub-laminar drag in a fully developed channel flow. *J. Fluid Mech.* **558**, 309–318.

Moarref, R. & Jovanović, M. R. 2006 Transition control using an array of streamwise vortices. In *Proceedings of the 45th IEEE Conference on Decision and Control*. San Diego, CA, to appear.

Nayfeh, A. H. & Mook, D. T. 1979 *Nonlinear oscillations*. New York: John Wiley & Sons.

Orlandi, P. & Fatica, M. 1997 Direct simulations of turbulent flow in a pipe rotating about its axis. *J. Fluid Mech.* **343**, 43–72.

Reddy, S. C. & Henningson, D. S. 1993 Energy growth in viscous channel flows. *J. Fluid Mech.* **252**, 209–238.

Schmid, P. J. & Henningson, D. S. 2001 *Stability and Transition in Shear Flows*. New York: Springer-Verlag.

Trefethen, L. N., Trefethen, A. E., Reddy, S. C. & Driscoll, T. A. 1993 Hydrodynamic stability without eigenvalues. *Science* **261**, 578–584.

Walsh, M. J. 1983 Riblets as a viscous drag reduction technique. *AIAA J.* **21** (4), 485–486.